Clim Dyn (2008) 30:657–671
DOI 10.1007/s00382-007-0315-0

Future changes in cyclone climatology over Europe as inferred from a regional climate simulation

P. Lionello · U. Boldrin · F. Giorgi

Received: 1 August 2006 / Accepted: 25 August 2007 / Published online: 26 September 2007

Abstract This study analyzes the cyclone climatology in regional climate model simulations of present day (1961–1990) and future (2071–2100, A2 and B2 emission scenarios) european climate conditions. The model domain covers the area from Scandinavia to Northern Africa and from the Eastern Atlantic to Russia at a horizontal grid spacing of 50 km. Compared to present day, in the A2 and B2 scenario conditions the annual average storm track intensity increases over the North-East Atlantic and decreases over Russia and the Eastern Mediterranean region. This overall change pattern is larger in the A2 than in the B2 simulations. However, the cyclone climatology change signal shows a large intermonthly variability and important differences across European regions. The largest changes are found over the North-East Atlantic, where the storm track intensity increases in winter and decreases in summer. A significant reduction of storm track intensity is found during late summer and autumn over the Mediterranean region, and from October to January over Russia. The number of cyclones decreases in future conditions throughout Europe, except over the Central Europe and Mediterranean regions in summer (where it increases). The frequency of intense cyclones and the depth of extreme cyclones increase over the North-East Atlantic, decrease over Russia and show an irregular response over the rest of the domain.

P. Lionello (✉)
Department of Material Science, University of Salento,
Via per Arnesano, Lecce, Italy
e-mail: piero.lionello@unile.it

U. Boldrin
University of Padua, Padua, Italy

F. Giorgi
ICTP, Trieste, Italy

1 Introduction

The frequency and intensity of extratropical cyclones are relevant for many environmental factors such as wind, precipitation, temperature, cloudiness, thunderstorms, floods, waves, storm surges, landslides, air quality and visibility (see Lionello et al. 2006a for a review). It is therefore important to identify changes of cyclone regimes and characteristics under possible future climate conditions.

In this study we investigate changes in cyclone regimes for an area encompassing the European region and ranging from the North-East Atlantic to the Red Sea. The North Sea, the British Islands and Central Europe are under the influence of the Mid-Latitude storm track. North Africa and the Middle East are affected by the descending branch of the Hadley cell. The southern portion of the region includes the Mediterranean Sea, which is surrounded by a complex structure of morphological features (Lionello et al. 2006b) leading to cyclogenetic processes associated with air–sea interactions, orographic and thermal effects (Lionello et al. 2006a). A heterogeneous response to future climate change scenarios can thus be expected in different areas of the region considered in this study.

Several studies have analysed present trends and future changes of cyclone frequency and intensity over the European region. The identification of cyclones from sea level pressure (SLP) data during the twentieth century reveals trends, large multidecadal variability and important regional patterns. For example, pressure time series at stations in

southern England indicate an increase in severe storms since the 1950s (Alexander et al. 2005). The analysis of pressure tendencies and very low pressure values extracted from two long time series (available since 1800) over southern Sweden shows a decline of cyclone activity during the late nineteenth century to a minimum around 1960, a subsequent strong increase with a maximum around 1990 and a following decline (Bärring and von Storch 2004). This is confirmed by an analysis of geostrophic winds based on pressure station values (Alexandersson et al. 2000). A counting of cyclones centres (Maheras et al. 2001) based on the NCEP re-analysis (Kalnay et al. 1996) shows a reduction of the number of cyclones in the western Mediterranean. A recent study analyzed the interannual variability of storm-tracks in the Euro-Atlantic sector in ERA-40 (Simmons and Gibson 2000) and NCEP/NCAR re-analyses for the December–March season between 1958 and 2000 (Trigo 2005). For both the ERA-40 and NCEP/NCAR data, two zonal bands were identified, one showing an increase in cyclone frequency from the Labrador Sea to Scandinavia and the other a decline from the Azores to Central Europe and the Mediterranean.

Therefore, most surface pressure-based studies suggest a northward shift and intensification of the winter mid-latitude storm-track over Europe during the second half of the twentieth century, which is consistent with the fluctuations observed during the last 40 years of the North Atlantic Oscillation (NAO), and its attenuation while propagating across northern Europe (Hurrel 1995; Ulbrich and Christoph 1999; Wang et al. 2006).

A number of studies have been carried out on cyclone statistics over Europe in global model simulations. In a doubled CO_2 simulation carried out with the ECHAM model at T106 resolution (about 1.1°), a small (but significant) decrease of the total number of Mediterranean cyclones and an increase of the number of intense cyclones was found by Lionello et al. (2002). In a transient simulation with the ECHAM4-OPYC3 model covering the period 1860-2100 and adopting the IS92a emission scenario, opposite signs of changes were found between Northern and Southern Europe (Pinto et al. 2006a). More precisely, for cyclones with high vorticity a 44% reduction over the Mediterranean region, and a 18% increase over the Eastern North Atlantic were found, along with a general decrease of the number of cyclones. A study based on four GCMs (ECHAM5/OM1, ECHAM4/OPYC3, HadAM3P, HadCM3) and five regional models for the SRES A2 scenario (Nakićenović et al. 2000) showed a decreased activity over central Europe and the Mediterranean region, but inconsistent changes at high latitudes (Leckebusch et al. 2006).

Two european projects (WASA and STOWASUS) analyzed trends and sensitivity to emission scenarios of marine storminess in European Seas. WASA reached the conclusion that the occurrence of storm surges and waves over most of the Northeast Atlantic and the North Sea has decreased during the central part of the twentieth century, with comparably higher levels in the earlier and later decades (WASA 1998). These wave height variations, and particularly an increasing trend in the last 4 decades of the twentieth century, have been confirmed by two recent studies using different wave re-analyses (Wang and Swail 2001; Wang and Swail 2002). STOWASUS (Kaas et al. 2001) found an increase of up to 10% in maximum surge values under future climate conditions for the west coasts of Jutland in Denmark. Multi-model wave height projections using SLP field projections show significant increase of mean seasonal values for winter, spring and summer (Wang and Swail 2006).

Concerning the Mediterranean, Lionello and Sanna (2005) found that wave heights have been decreasing in various parts of the Mediterranean sea during the second half of the twentieth century. Lionello (2005) identified large interdecadal fluctuations, but no clear trends, in extreme storm surges over the Adriatic Sea. Double CO_2 simulations indicated a reduction of extreme wave heights, but no clear trend in storm surge levels (Lionello et al. 2003). Finally, Lionello et al. (2007) used wind fields computed by regional climate simulations[1] for the period 2071–2100 to find a reduction of wave height in November, December and May under increased greenhouse gas (GHG) forcing.

In summary, the bulk of evidence from recent studies mostly supports, or at least does not contradict, the finding of an attenuation of cyclones over the Mediterranean and an intensification over Northern Europe during the second part of the twentieth century. It also suggests that this trend would continue as a consequence of future increased GHG forcing.

Here we investigate changes in cyclone statistics over Europe from two regional climate model simulations for different GHG emission scenarios. This allows us to use data with higher spatial resolution than in previous studies and therefore offers an ideal framework for evaluating the presence of contrasting trends in the change signals at small spatial scales. Moreover, we consider two GHG emission scenarios (the IPCC A2 and B2 scenarios), which allows us to estimate the dependence of the change signal on the GHG forcing. Finally, we analyze the whole annual cycle rather than focusing on specific seasons, and investigate the intensity of extreme events.

The data and analysis methods used in his study are described in Sect. 2. Section 3 discusses the mean cyclone

[1] The wind fields were produced by the same simulations analyzed in this study, see Sect. 2 for information

change signal over the entire area considered. This is then divided into four regions (NEA North East Atlantic, SCA SCAndinavia, RUS RUSsia, CEM Central Europe and Mediterranean, Sect. 4) on the basis of a PCA (Principal Component Analysis). The different characteristics of the response to future emission scenarios in these four regions are discussed in Sect. 5. Section 6 discusses the significance and robustness of the change signals and summarizes the main results of this study.

2 Data and methods

In this study we analyze three 30-year regional climate simulations, one for present day conditions (1961–1990) (CTR experiment) and two for future conditions (2071–2100) under the A2 and B2 IPCC emission scenarios (Nakićenović et al. 2000). The A2 is a high emission scenario, lying towards the high end of the IPCC range, while the B2 is a low emission scenario lying towards the low end of the range. The simulations are carried out with the regional climate model RegCM (Giorgi et al. 1993a, 1993b; Pal et al. 2000) driven at the lateral boundaries by meteorological fields from the Hadley Centre global atmospheric model HadAM3H (1.25×1.875 lat-lon horizontal resolution) (Jones et al. 2001). Sea surface temperatures (SSTs) are from corresponding simulations with the Hadley Centre global coupled model HadCM3 (Jones et al. 2001). The model grid spacing is 50 km and the model domain covers the European region and adjacent oceans as shown in Fig. 1. For more information on the model and for a general discussion of the simulations, the reader is referred to Giorgi et al. (2004a, 2004b). In this study we analyse 6 h SLP (Sea Level Pressure) fields from these three 30-year simulations.

Two different approaches are used to analyze the cyclone activity: a "lagrangian" approach based on a cyclone trajectory identification algorithm and an "eulerian" approach based on the computation of the SLP standard deviation. The lagrangian approach adopts the procedure by Lionello et al. (2002), which identifies the location where each cyclone originates and follows the trajectory of its pressure minimum until it disappears from the SLP maps. The procedure produces a list of cyclones, along with the position and value of the SLP minima. The results of cyclone detecting algorithms are very sensitive to the resolution of the analysed fields in terms of number and intensity of cyclones identified. In general, the number of detected cyclones increases with resolution (e.g., Pinto et al. 2006b). Moreover the southern part of the model

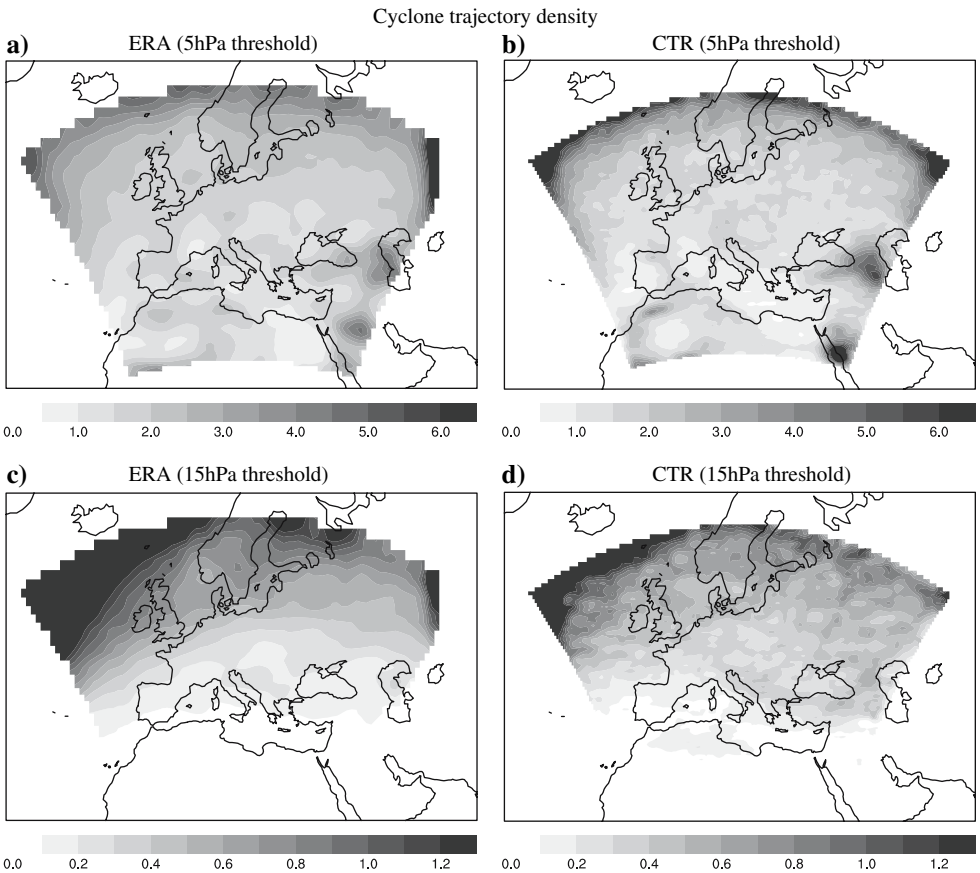

Fig. 1 Density of cyclone trajectories (unit 10^6 number of trajectories km^{-2} month^{-1}, only cyclones with duration longer than 1 day are considered). In panels **a** (*ERA*) and **b** (*CTR* simulation) all cyclones deeper than 5 hPa are included, in **c** (*ERA*) and **d** (*CTR* simulation) cyclones deeper than 15 hPa are included

domain includes cyclones with limited extension (radius often smaller that 500 km) which are not resolved by low resolution global models (see Lionello et al. 2006a for a discussion of cyclone tracking algorithms in the Mediterranean area). Figure 1 shows the average monthly frequency of cyclone trajectories for the whole CTR simulation and for the ERA re-analysis. The map shows the average density of trajectories which, integrated over a given area, gives the monthly average number (or fraction) of trajectories inside the area and when integrated over the whole domain gives the total number of identified trajectories. Figure 1a and b consider all cyclones with a depth exceeding 5 hPa, while Fig. 1c and d consider cyclones with a depth exceeding 15 hPa. Before the application of the cyclone tracking algorithm, both sets of data are preprocessed with a bandpass (1–7 days) Lanczos digital filter. The comparison with the ERA re-analysis shows that the CTR simulation reproduces well the main features of the ERA data, including the spatial distribution of the cyclone frequency. Note that the CTR fields have a higher resolution than the ERA data. This probably plays a role in determining the differences of cyclone numbers (larger in the CTR than in the ERA fields) over the southern part of the domain, where cyclones have a smaller extension and are shallower than in the north. Most cyclogenetic areas, such as in the southern side of the Alps, are present in both maps. The CTR simulation largely overestimates the number of cyclones close to the Caspian Sea, an area probably too close to the border of the model domain to be realistically simulated, and underestimates the number of cyclones in the North East Atlantic.

The Eulerian approach applies a band-pass filter to the SLP field (the Lanczos filter), which retains the variability in the 1–7 days period, and computes the SLP standard deviation. For brevity, we call the standard deviation of the band pass filtered SLP fields "synoptic signal". The prominent features of the geographical distribution of this quantity are often called "storm tracks" in the literature. The lower cut-off value can marginally penalize the signal produced by cyclones in the Mediterranean region, where the time scales of cyclone development are shorter than in northern Europe and the Atlantic region. In general, however, short-lived weather disturbances and daily characteristics of weather events are not within the scope of this study. In addition, the application of the cyclone tracking algorithm is restricted to the band-pass filtered fields. As a result, only major and persistent features are considered here and the depth of cyclones is evaluated with respect to a slowly evolving background field. Figure 2a and b show the average monthly synoptic signal for the ERA reanalysis and the CTR simulation. Well-known features of the North Atlantic storm track, such as its penetration over northern Europe across Scandinavia and towards Russia and its southern branch over the Mediterranean Sea, are evident in the CTR simulation. This agrees with the ERA data. For both the synoptic signal and the cyclone frequency, the CTR simulation presents an overestimation in the southern part of the domain and an underestimation in the northern part.

3 The overall climate change signal in Europe

Figure 3 shows the cyclone activity over the entire analysis region in the three simulations (CTR, A2, B2) and the results of the Mann-Whitney (MW) test for the assessment of the statistical significance of the differences between the CTR and the A2 and B2 results. The advantage of the MW test is that it is non parametric, i.e., it only requires that the deviations of two samples denoted as X_i, $i = 1,...,N_X$ and Y_j, $j = 1,...,N_Y$, from the relative mean $X_i - \langle X \rangle$ and $Y_j - \langle Y \rangle$ have the same distribution without specific assumptions on the shape. The values X_i and Y_j assumed by the variable in the two samples are set in decreasing order and the rank R_X of X is defined as the sum of the positions of the relative values in the list. Note that higher ranks are given to samples with lower values. It can be proven that the dimensionless variable

$$S_X = \frac{R_X - N_X(N_X + N_Y + 1)/2}{(N_X N_Y (N_X + N_Y + 1)/12)^{1/2}} \quad (1)$$

has a Gaussian distribution with zero mean and unit variance if N_X and N_Y are sufficiently large, which is true for our study employing 30 years of data (von Storch and Zwiers 1999). In practice, values of S_X higher (lower) than ±1.645 (shown by the horizontal lines in the right panels of Fig. 3 and of following similar figures) imply that the values X_i are significantly lower/higher than Y_j at the 95% confidence level.

Figure 3a shows the annual cycle of the SLP monthly synoptic signal for the entire analysis domain. The vertical bars denote the standard deviation of the monthly values. The annual cycle has a simple structure with a maximum in winter and a minimum is summer. Figure 3b shows the result of the MW test comparing the A2 and B2 experiments with CTR. A clear change signal can be identified in the A2 scenario, consisting of a reduction of the SLP synoptic signal from August to November. In the B2 scenario the reduction is significant only in August.

Figure 3c and d show the annual cycle of the monthly number of cyclones, the corresponding standard deviation and the MW test. The counting includes only cyclones with a duration of at least 1 day and whose central minimum reaches a value deeper than 5 hPa at least in one filtered SLP field. Note that the number of cyclones has a

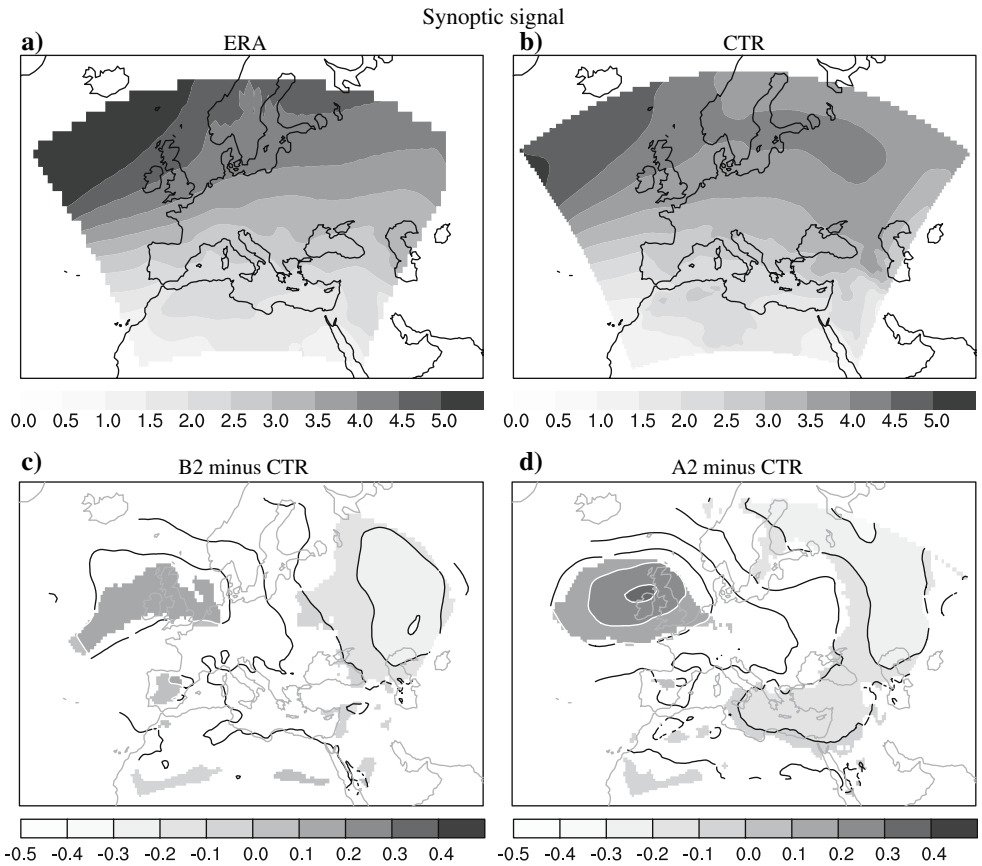

Fig. 2 Average synoptic signal in ERA re-analysis (panel **a**, values in hPa) and *CTR* simulation (panel **b**). Average synoptic signal differences between scenario simulations and *CTR*: B2 scenario (panel **c**) and A2 scenario (panel **d**). Positive values denote areas where the scenarios are higher than *CTR*. The *bold contours* denote the zero-level. Contour levels according to the *bar* below each panel. *Shading* indicate differences which are significant at the 95% confidence level. All panels are derived from the band-pass filtered fields

maximum in summer (when the cyclone frequency is about 20% higher than in winter), while the synoptic signal has a minimum is summer (when the average value is about 50% lower than in winter), so that the average synoptic signal per cyclone (Fig. 3e) is much lower in summer than in winter (the reduction is about 60%). The cyclone change signal is largest in the A2 scenario, with a significant decrease of the cyclone frequency in December and January and an increase in September. It will become clear in Sect. 4 that the absence of a change signal in summer is actually the result of opposite trends between different regions of the domain. In the A2 scenario opposite changes in cyclone frequency and monthly synoptic signal combine so that the average SLP synoptic signal per cyclone significantly increases in December and January, and decreases in August and September (Fig. 3, bottom panels). Though also high pressure systems contribute to the synoptic signal, these changes suggest a corresponding increase/decrease of the average strength of cyclones.

The shape of the annual cycle of cyclone frequency depends on the threshold used for counting cyclones. If cyclones whose central minimum reaches values deeper than 10 hPa are considered (top panels of Fig. 4), the maximum cyclone frequency moves from August to March. If the threshold is further increased to 20 hPa, the maximum moves to January and the annual cycle becomes similar to that of the synoptic signal. The cyclone frequency change signal also depends on the SLP threshold. As the threshold increases (i.e., more intense cyclones are considered) the differences between scenarios and CTR cyclone frequencies decrease and the tendency for the scenarios to produce a lower cyclone frequency incrementally disappears. For example, if cyclones deeper than 10 hPa are considered, the A2 and B2 scenario simulations show fewer cyclones than the CTR for most months, with the differences being quite large and significant from November to January and in July (Fig. 4b). If cyclones deeper than 20 hPa are considered (this choice excludes weak cyclones and retains moderate and strong cyclones) only September shows a significant frequency reduction in both scenarios (Fig. 4d).

The dependence of the changes in cyclone frequency on the cyclone intensity is clear when considering the distribution of the average monthly number of cyclones as a function of depth (Fig. 5). This is defined as the maximum depth reached during the whole lifetime of each cyclone in the band-pass filtered SLP fields. The left panel shows the distribution in the range of weak and moderate cyclones, from 5 to 20 hPa, and it presents a clear reduction of weak cyclones in future climate conditions, which is larger in the A2 than in the B2 scenario. The right panel, which considers the upper tail of the distribution (from 20 to 35 hPa)

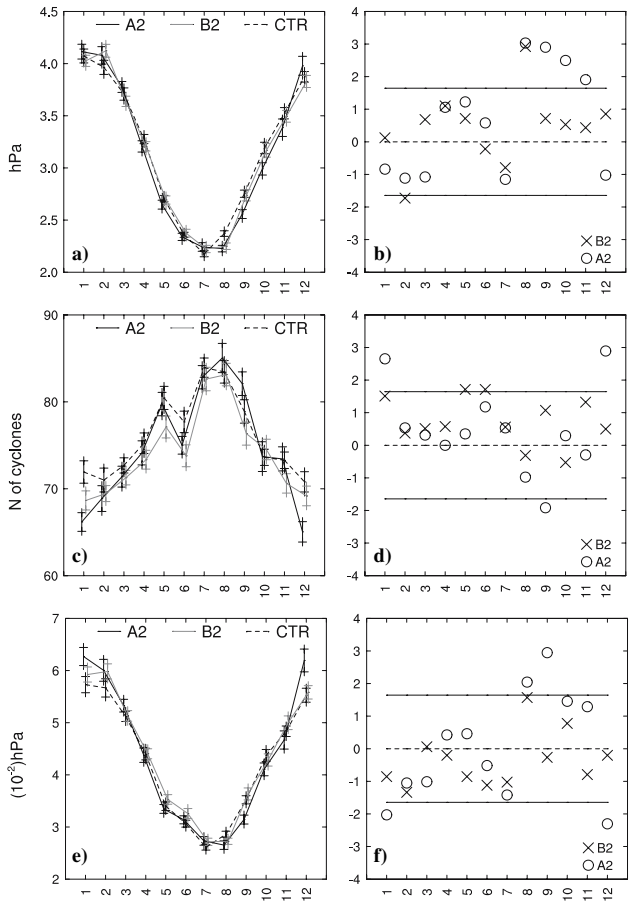

Fig. 3 Annual cycle of synoptic signal over the whole area (units hPa, panel **a**), of cyclone frequency (panel **c**, all cyclones deeper than 5 hPa are included), of synoptic signal normalized with the number of cyclones (panel **e**). Calendar months on the x-axis. The *vertical bars* show the corresponding standard deviations. *Black*, *grey* and *dashed line* refer to A2, B2, and CTR respectively. The panels **b**, **d** and **f** (on the right column) show the results of the respective MW test. The *horizontal lines* mark the limit for the 95% confidence level. In all panels calendar months are shown on the x-axis

shows little change for moderate cyclones and larger frequency of intense cyclones in the two scenario experiments (particularly in the A2).

A GEV (Generalized Extreme Value) analysis confirms that the intensity of extreme cyclones increases in the A2 and B2 scenarios. The values of the three deepest cyclones of each month have been used to estimate the three parameters of the GEV distribution. Figure 6 shows the annual cycle of the resulting 50-year return values for the CTR and scenario simulations. Both the A2 and B2 scenario runs show higher extreme cyclone values in November and December than CTR and lower values in August. However, note that only a few of the variations of the monthly extreme values are significant if statistical uncertainties (shown by the *bars* in Fig. 6) are accounted for.

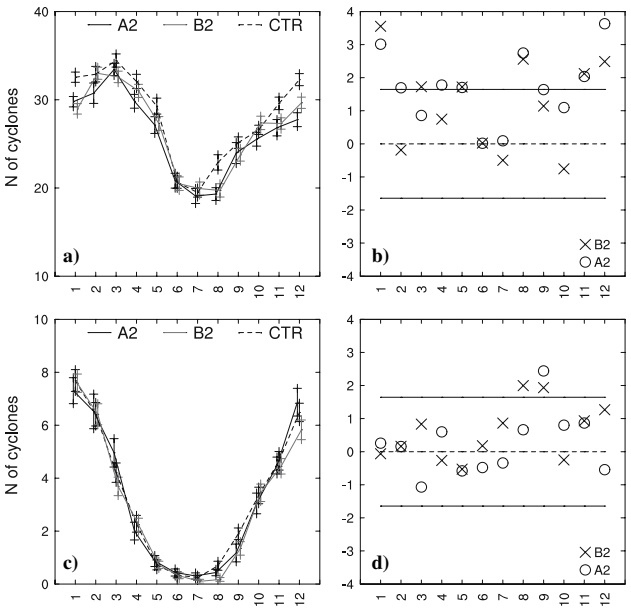

Fig. 4 Annual cycle of the monthly frequency of cyclones (panels **a** and **c**) and MW test statistics (panels **b** and **d**). Calendar months on the x-axis. *Top* and *bottom rows* consider cyclones with a maximum depth larger than 10 and 20 hPa, respectively. *Black*, *grey* and *dashed line* refer to A2, B2 and CTR, respectively

4 Regional characterization of the cyclone change signal

Figure 2c and d show large differences across Europe in the cyclone change signal. The SLP synoptic signal increases over the North-East Atlantic and British Islands and decreases over Russia and the Eastern Mediterranean. In addition, the warm and cold seasons show different change signals (e.g., Fig. 3a, b). Therefore it is important to evaluate the spatial and seasonal distributions of the

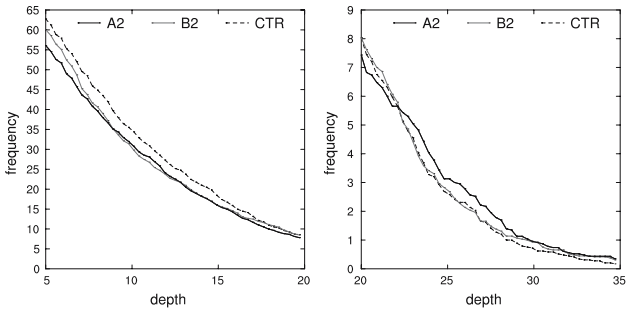

Fig. 5 Dependence of the average monthly number of cyclones on depth which is defined as the maximum depth reached during the whole lifetime of each cyclone in the band-pass filtered SLP fields. The figures show the monthly average number of cyclones (y-axis) exceeding a given depth (x-axis, units hPa). The *left panel* shows the distribution in the range from 5 to 20 hPa, the *right panel* in the range from 20 to 35 hPa. *Black*, *grey* and *dashed line* refer to A2, B2 and CTR, respectively

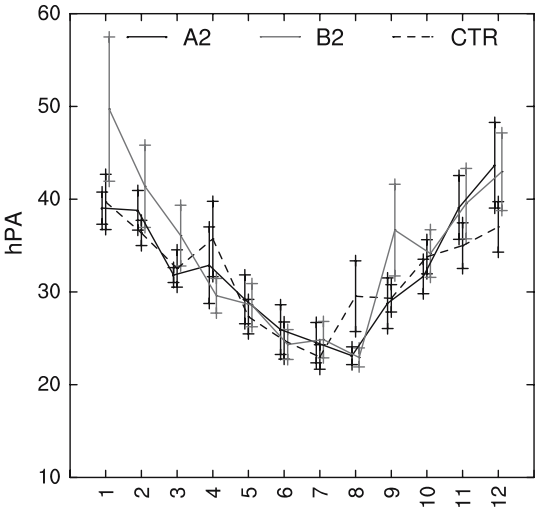

Fig. 6 Results of the GEV analysis for the whole model domain: annual cycle (calendar months on the x-axis) of cyclone depth (y-axis, units hPa) corresponding to the 50-year return time

cyclone statistics. Towards this purpose, a PCA of the SLP monthly synoptic signal field was carried out in order to identify regions characterized by a coherent variability.

The first EOF (Empirical Orthogonal Function, Fig. 7a) of the synoptic signal is clearly dominant in describing the temporal variability of the fields (Table 1). This is associated with an overall cycle of intensification/attenuation of the storm track over Europe, with an opposite sign occurring only over a small area of North Africa. It corresponds to the cold–warm season signal, having a maximum in December–January (Fig. 8a) and a minimum in July–August.

In order to associate each EOF with the spatial distribution of cyclones, composites showing the density of cyclone trajectories in months with high (Fig. 7d, g) values of the corresponding PC (Principal Component) were computed. The composites include the upper/lower 10% of the PC values. Each figure shows the monthly average density of cyclone trajectories which, similarly to Figure 1, has been smoothed by aggregating over boxes consisting of 25 model cells and multiplied by a factor of 10^6. The cyclone center density shows that high/low values of the first PC (Principal Component) are associated with high/low numbers of cyclone trajectories over the entire European domain.

The second EOF (Fig. 7b) describes a shift of the mid-latitude storm track. The corresponding explained variance

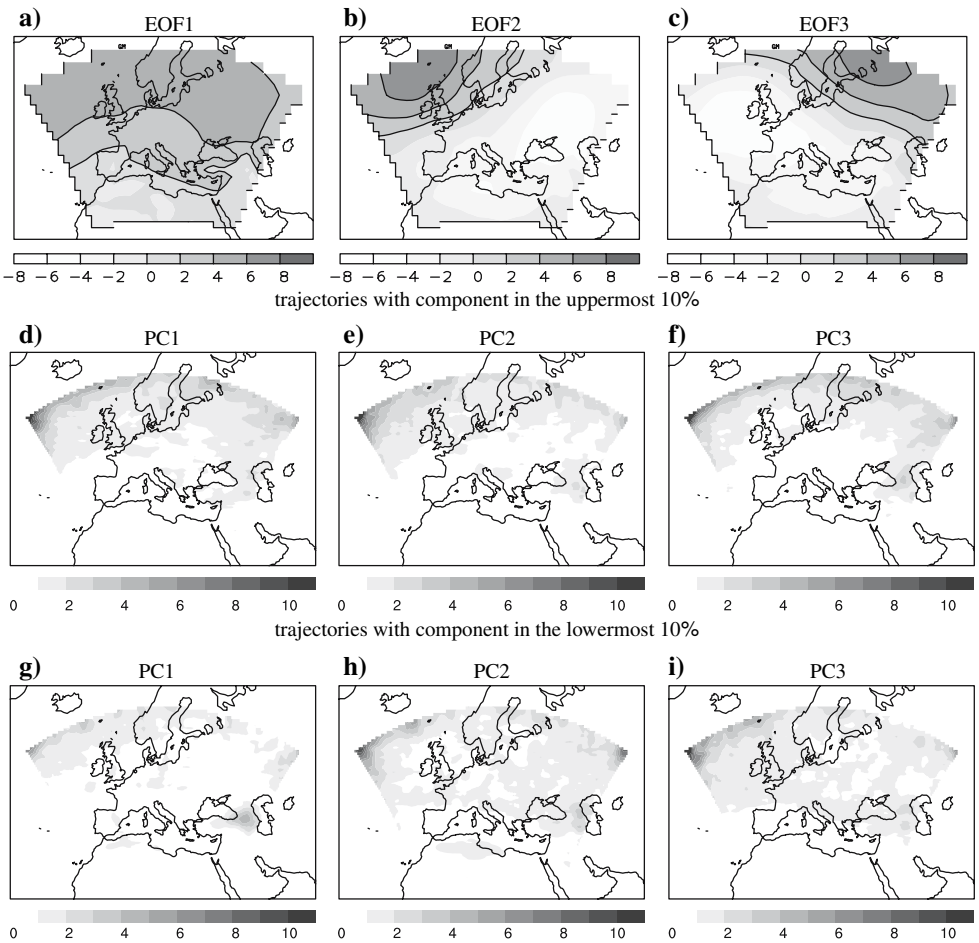

Fig. 7 Association between the structure of the leading EOFs (panel **a**–**c**, values normalized with the respective maxima, *black/white contour lines* denote positive/negative values) and the density of cyclone center trajectories conditioned on the values of the leading PCs. The first, second, and third column refer to the first, second, and third EOF, respectively. *Middle* (*bottom*) *row* shows the trajectory density for the months with the respective PC in the 10% upperemost (lowermost) range. Only cyclones deeper than 10 hPa and with duration longer than 1 day are included (units 10^6 number of trajectories km^{-2} month^{-1})

Table 1 Eigenvalues and percentage of explained variance for the first three EOFs of the monthly synoptic signal in the CTR, A2 and B2 simulations

	CTR			B2			A2		
	First	Second	Third	First	Second	Third	First	Second	Third
Eigenvalue	616	99	72	537	127	69	533	103	80
Percentage	60.0	9.7	7.1	54.9	12.9	7.0	55.6	10.7	8.3

is much lower than for EOF1 (Table 1). It presents a dipole with centers above the north-eastern Atlantic and southern Russia, splitting the model domain along a nodal line oriented from the south-west to the north-east which separates two areas where the synoptic signal has opposite signs. Correspondingly, the cyclone center density is high in the north-western (eastern) part of the analysis area in correspondence of positive (negative) values of the second PC. The second PC has a well defined annual cycle (Fig. 8b). Over the north-western Atlantic the signal intensifies in spring (March–April) and attenuates in autumn (September–October). The opposite occurs over Russia.

The third EOF (Fig. 7c) describes the variability of the direction of the storm track during its penetration over Europe. It splits the model domain in two parts along a nodal line oriented from the north-west to the south-east. The corresponding dipole has a center over the eastern Atlantic and Scandinavia, while the density of cyclone centers is high over the eastern Atlantic and Mediterranean (or Scandinavia and Russia) for high (or low) values of the third PC. It appears that intensification/attenuation of the storm track over the Western Europe-Mediterranean and the Scandinavia-Russia regions are out of phase. The EOF3 and EOF2 have comparable values of explained variance, and the annual cycle of the third PC (Fig. 8c) has a phase quite different from that of the second PC, so that the two components of variability partially compensate each other in some areas.

Differences of shape of the EOFs and of the corresponding PC annual cycles between the A2, B2 and CTR simulations do not appear important, so that the previous description is valid also for the A2 and B2 scenarios. Accordingly, the whole area is divided into four regions by the two intersecting lines approximating the nodal lines of the second and third EOF (Fig. 9): NEA (North East Atlantic), RUS (RUSsia), CEM (Central Europe and Mediterranean), SCA (SCAndinavia).

5 Regional scale differences across Europe

As shown in Fig. 2 and consistently with the characteristics of the annual cycle described in the previous Sect. 4, the differences in synoptic signal between the future scenario simulations and the CTR are not spatially homogeneous. Moreover, intermonthly variability is important. The annual cycle of the spatial distribution of the statistically significant differences of the synoptic signal between the A2 or B2 and the CTR simulations is shown in Figs. 10 and 11, respectively (positive values indicate that the scenario simulations have larger values). The MW test was used to assess the significance of the changes, and only regions where the changes are significant at the 95% confidence level are shaded.

Common features are present in both scenarios, with large changes being generally associated with stronger GHG forcing (i.e., larger changes in the A2 than the B2 simulation). Among these features are an increase of the synoptic signal from December to March and a decrease in August over the British Islands; an increase over Russia in July; a small decrease over part of the Mediterranean from August to November (much larger for the A2 than the B2 scenario).

Calculations of the synoptic signal and cyclone number, along with the analysis of extreme cyclones, have been performed separately for the NEA, SCA, RUS and CEM regions and are discussed below.

5.1 North-East Atlantic

North-East Atlantic (NEA) is the region where the largest change of cyclone statistics is observed. The overall number of cyclones is smaller in the A2 and B2 scenarios than in the CTR and, conversely, intense cyclones are more frequent (Figs. 12a, b; 13a, b). The monthly cyclone numbers (Fig. 14c, d) are smaller in the scenario experiments than in CTR in all months (note that this variable has a weak intermonthly variability both in the scenario and CTR simulations). However, if cyclones stronger than 20 hPa are considered (Fig. 14e, f), all simulations show a large and similar annual cycle, with no significant differences except for a decrease of cyclone number in the scenario simulations during late summer.

The synoptic signal tends to increase from October to May and decrease in August (Fig. 14a, b). For some months (January, February, August) the changes are well above the 95% confidence threshold in both scenarios.

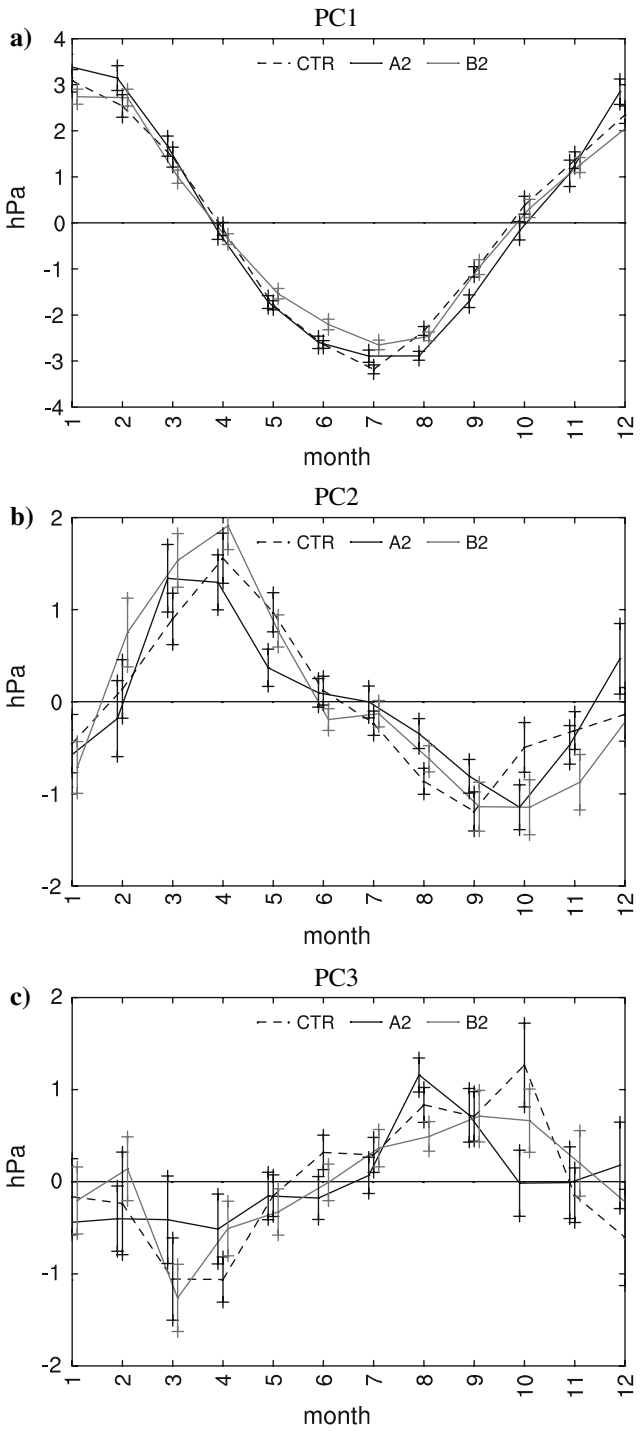

Fig. 8 Annual cycles (calendar months on the x-axis) of the leading PCs (units hPa) in the CTR, A2 and B2 scenario simulations. First, second and third PC in the **a**, **b** and **c** panel, respectively

A GEV analysis (Figure 14g) suggests more intense extremes in the future scenario conditions for November and December and milder extremes in August. Other months show a more irregular behaviour of the changes in the A2 and B2 simulations compared to the CTR.

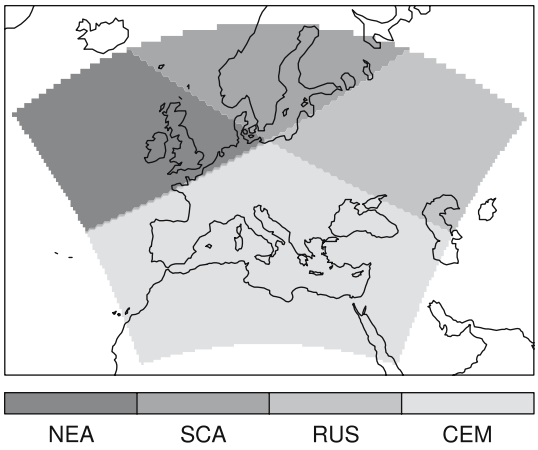

Fig. 9 The four regions selected for the analysis

5.2 SCAndinavia

In the SCAndinavian region the overall number of cyclones is reduced in both the A2 and B2 scenarios and, at the same time, intense cyclones are more frequent (Figs. 12b, 13b).

Summer appears to be the season most affected by the GHG forcing in both scenarios, with a lower synoptic signal in August, fewer cyclones from June to September and fewer intense cyclones (above the 15 hPa threshold) in September for the scenario simulations compared to the CTR (Fig. 15). The cyclone change signal is larger in the A2 scenario, where the reduction of the synoptic signal continues in autumn (October–November) and the number of intense cyclones decreases also in October. Note that for SCAndinavia (and for the RUS and CEM regions as well, see below) the threshold for considering intense cyclones has been reduced to 15 hPa in order to include a sufficient number of cyclones.

We also note that most characteristics of the cyclone change signal (as measured by both the synoptic signal and the cyclone density) in the SCA region (Fig. 15) are similar to those in the NEA region, except for an increase of the synoptic signal during the cold season in the NEA region (Fig. 14).

5.3 RUSsia

In the RUSsia region the synoptic signal is significantly and consistently lower in both scenarios than in the CTR (Fig. 16a, b) from October to May, although with a somewhat irregular intermonthly behaviour.

The overall number of cyclones tends to decrease in the scenario simulations, (Fig. 12c). Considering the monthly values, the difference compared to CTR is

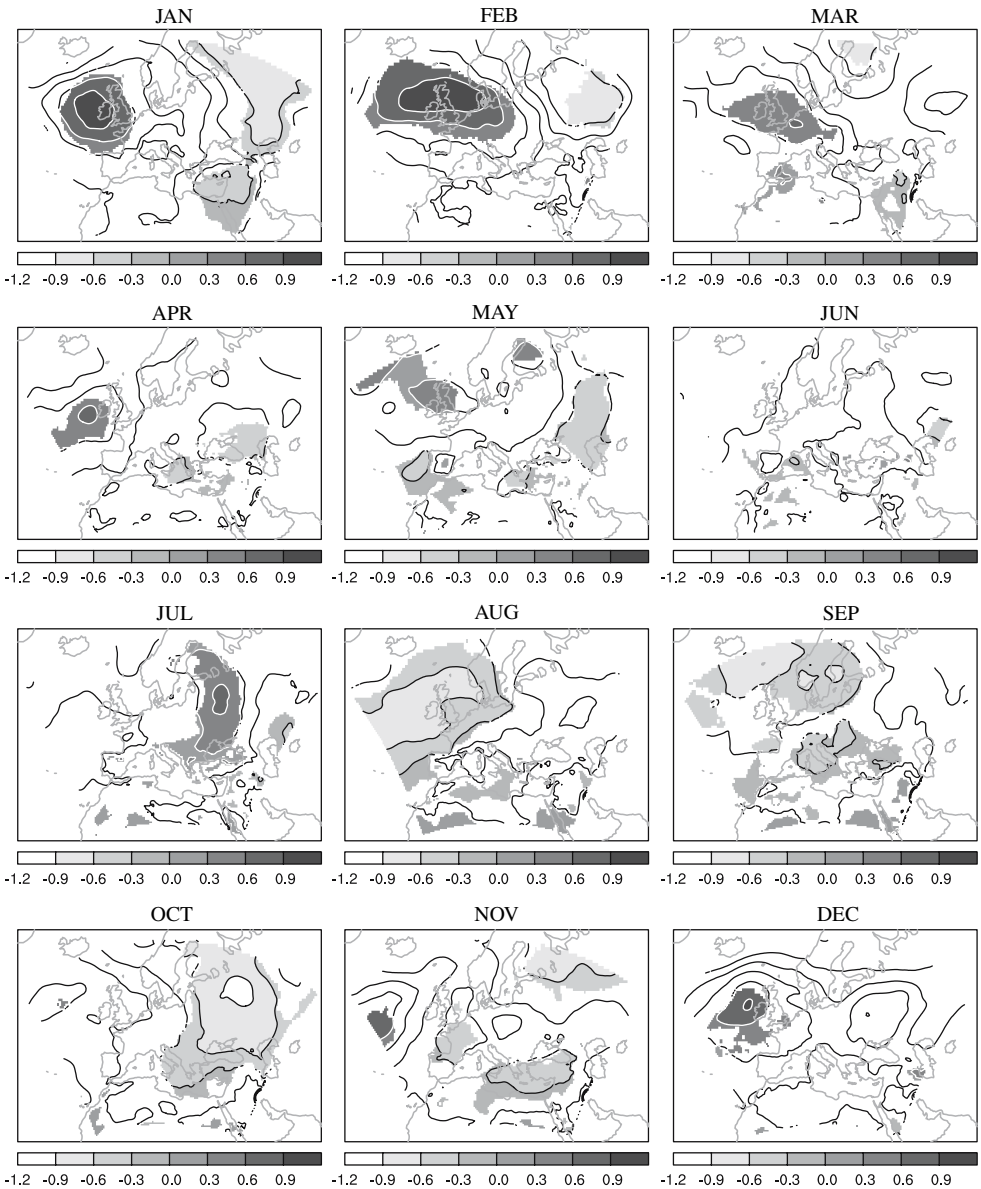

Fig. 10 Annual cycle of synoptic signal difference between A2 and CTR. Positive values denote areas where A2 is larger. Only areas where differences are significant at the 95% confidence level (the MW test has been used) are *shaded*

significant in March, May and November for both scenarios and from November to January in the A2 scenario (Fig. 16c, d). Differently from the NEA and SCA regions, in the RUS region the reduction of the frequency of cyclones occurs also for intense cyclones (Fig. 13c). Milder extremes occur in January and April (Fig. 16g) in both scenarios.

5.4 Central Europe and the Mediterranean

Considering the cyclone counting, the CEM region is the least affected in the climate change simulations (Figs. 12d, 13d). No appreciable differences are found in the B2 scenario experiment compared to the CTR, while a small overall reduction is suggested by the A2 scenario simulation, which is not confirmed for intense cyclones (Fig. 13d).

The synoptic signal of the A2 scenario run (Fig. 17a, b) shows a significantly decreased activity over the entire region in the periods September–November and April–May. For the B2 scenario the decrease is significant only in November. Monthly average values of cyclone frequency are not consistent with a reduction in synoptic activity. There is a tendency towards more cyclones in July and August (and also in September for A2) and less cyclones in December (and also January for A2, Fig. 17c, d). Compared to the CTR, extreme cyclones in both scenario simulations become stronger in March and weaker in April and August (Fig. 17g).

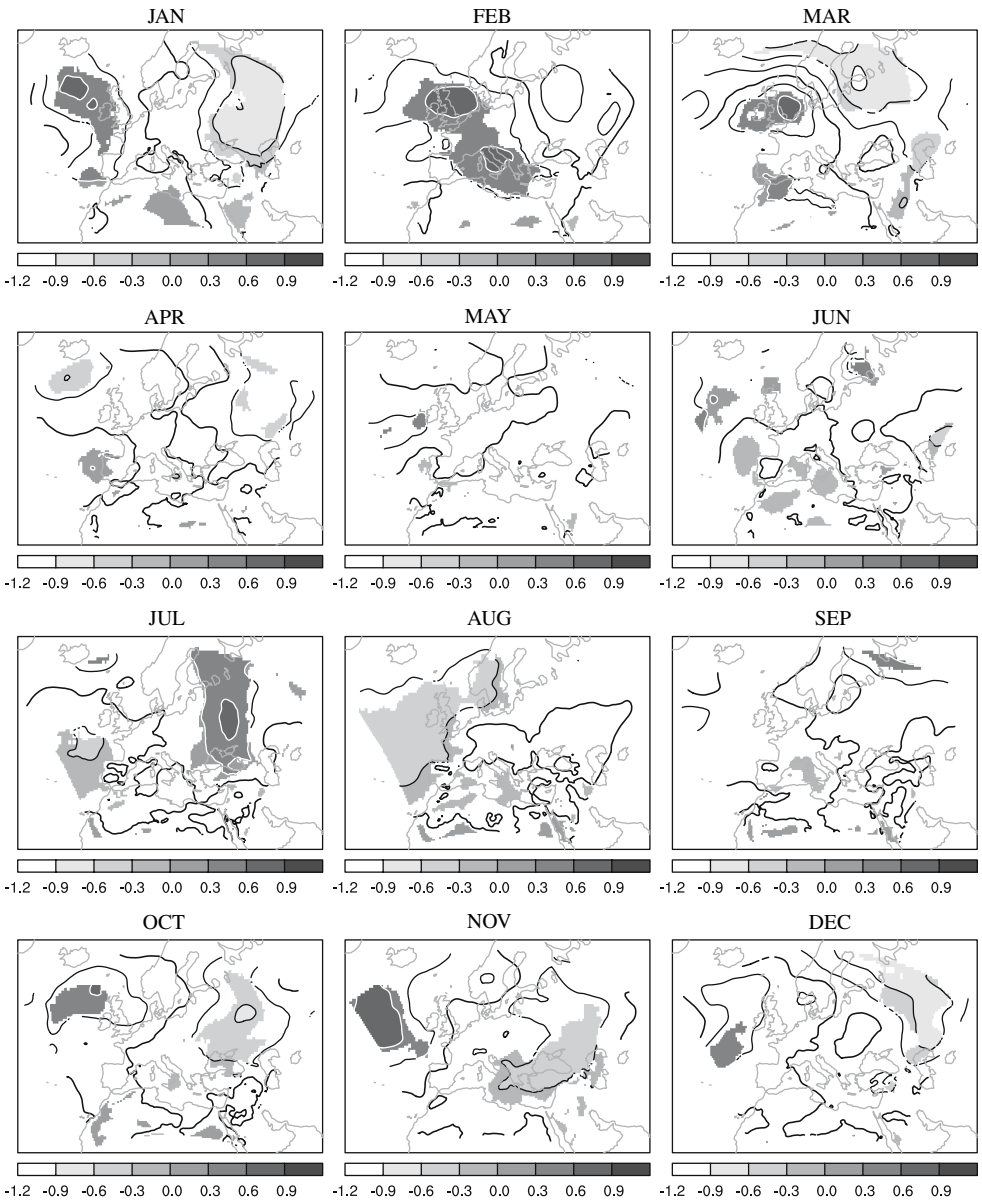

Fig. 11 As previous Fig. 10, but the differences between B2 and CTR are shown

6 Discussion and conclusions

Obviously, there are errors in the model and in the cyclone counting procedure which can affect the identification of cyclones and the resulting statistics. These errors are largest near the northern and southern boundary of the domain. For instance, considering the NEA region, the CTR simulation underestimates the synoptic variability (by about 15%) and the number of cyclones above the 15 hPa threshold (by about 25%), and overestimates the number of all cyclones above the 5 hPa threshold (by about 25%).

Moreover, several features of the simulated cyclone changes resulting from this analysis are noisy, they change sign in successive months and are not coherent in the two scenarios, although they are eventually statistically significant. This indicates a strong spatial and temporal variability in the cyclone change signal across Europe. Certainly, the regional European climate is characterized by an intrinsic variability which is superimposed to the change signal and it might occasionally counterbalance or magnify it.

It is therefore important to discuss the separation between "signal" and "noise" and the robustness of the projected changes. Ultimately, increased confidence in projected changes can be achieved by multiple simulations and analysis tools. However, even within our single model study some criteria for robustness can be suggested. One is

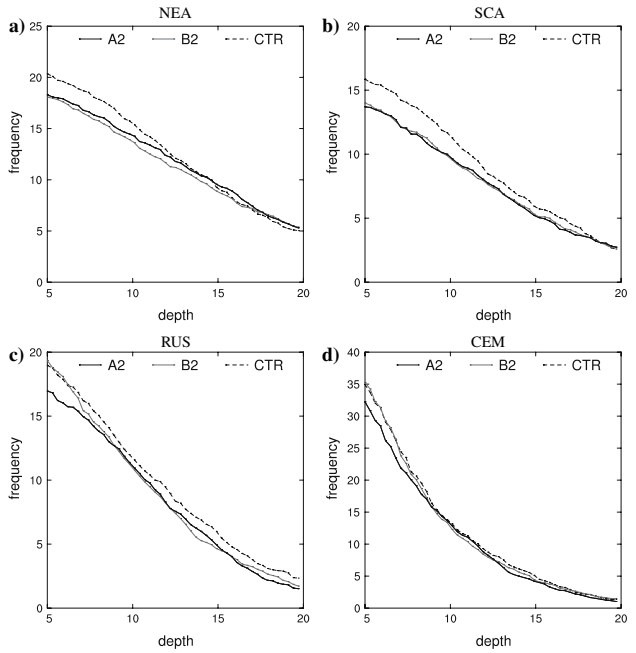

Fig. 12 Frequency (average monthly number) of cyclones (y-axis) exceeding the given depth (y-axis, hPa) (**a**) NEA region, (**b**) SCA region, (**c**) RUS region, (**d**) CEM region. The range from 5 to 20 is considered

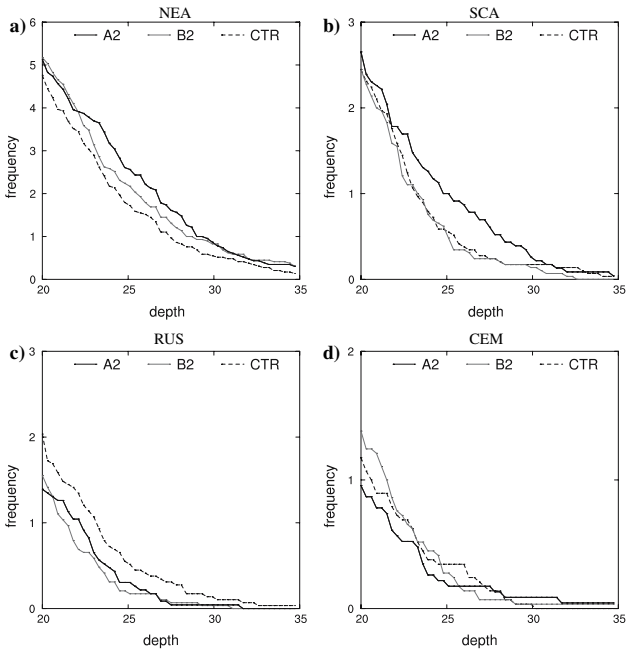

Fig. 13 As for Fig. 12, except that the range from 20 to 35 hPa is considered

the consistency between the signals in the A2 and B2 scenario simulations, with the magnitude of the signal being greater in the A2 than in the B2 scenario and thus implying a direct dependence on the GHG forcing. Another is the regularity of the intermonthly behavior, suggesting that the signal can be interpreted as coherently affecting the annual cycle, or portions of it, rather than being present only in isolated months (possibly from the contribution of noise). If we apply these criteria to features detected with a confidence level higher than 95% (this is, admittedly, a "conservative" approach) we can summarize the following list of "robust" signals:

6.1 Synoptic signal

- Increase from December to March and decrease in August and September in a region centered over the British Islands.
- Decrease over Russia in October, November and January.
- Small decrease in the Mediterranean region from August to November.

Note that these conlusions are based on the maps of synoptic signal shown in (Fig. 2). If the average time cycle is considered (Figs. 14–17) some details are slightly different, but the basic picture does not change. Moreover, we note an increase of the July synoptic signal over Russia which, although occurring only in 1 month, is quite large in both scenarios.

6.2 Overall number of cyclones

- Decrease of the yearly total number of cyclones everywhere except over the Central Europe and Mediterranean regions.
- Decrease in the North-East Atlantic region throughout the year except for September.
- Decrease in the Scandinavian region from June to September.
- Increase in the Central Europe and Mediterranean region in July and August.

Note that in March, May and November, there is a large reduction of the number of cyclones over Russia in both scenarios.

6.3 Intense cyclones

- Decrease of the average annual frequency of intense cyclones over Russia—lower number of cyclones deeper than 20 hPa in the North-East Atlantic region in August and September. There is no uniform robust signal for the monthly frequency of cyclones deeper

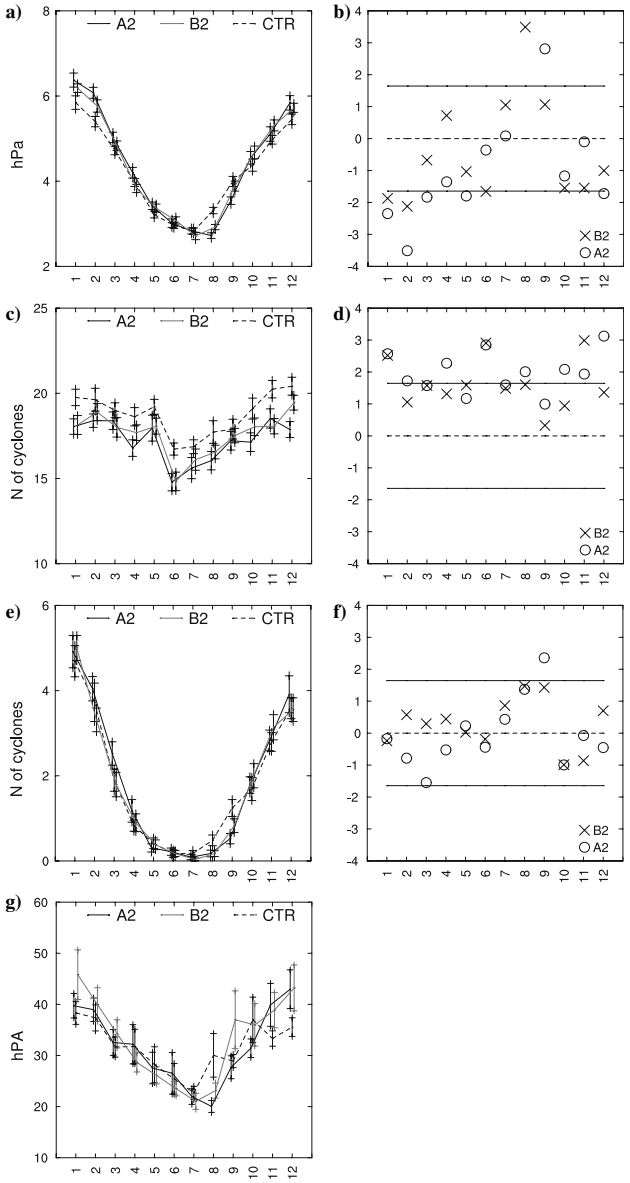

Fig. 14 NEA region annual cycle of synoptic signal (panel **a**, units hPa, calendar months on the x-axis), frequency of all cyclones deeper than 5 hPa (panel **c**), frequency of cyclones deeper than 20 hPa (panel **e**), along with the respective MW test statistics (*right column*, panels **b**, **d** and **f**). Panel **g** shows the annual cycle of cyclone depth (y-axis, units hPa) corresponding to the 50-year return time with the respective *error bars*

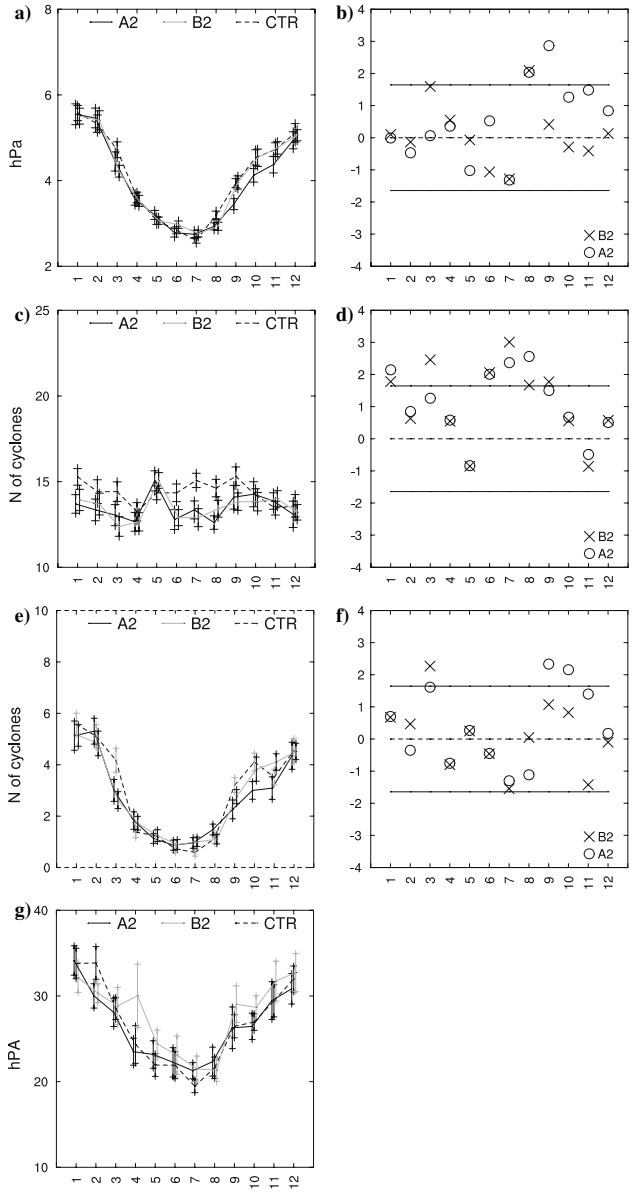

Fig. 15 Same as previous Fig. 14, except that the results for the SCA region are shown, and the threshold used for panels **e** and **f** is 15 hPa

than 15 hPa in the other regions. An eventual change signal is probably masked by the presence of large statistical fluctuations related to the small number of occurrences.

6.4 Extreme cyclones

- Increase in the North-East Atlantic region in November and December based on the GEV analysis.

We also note other results that do not satisfy the criteria above, but are worth being mentioned:

- Weaker extremes in April in both the Russia and Mediterranean regions.
- Weaker extremes in January over Russia (consistent with the decrease of intense cyclones).
- Weaker extremes in August in the North-East Atlantic region (consistent with the decrease of intense cyclones).

Our findings are consistent with the poleward shift of the mid-latitude storm track which most studies show in scenario simulations for both hemispheres (e.g., Ulbrich

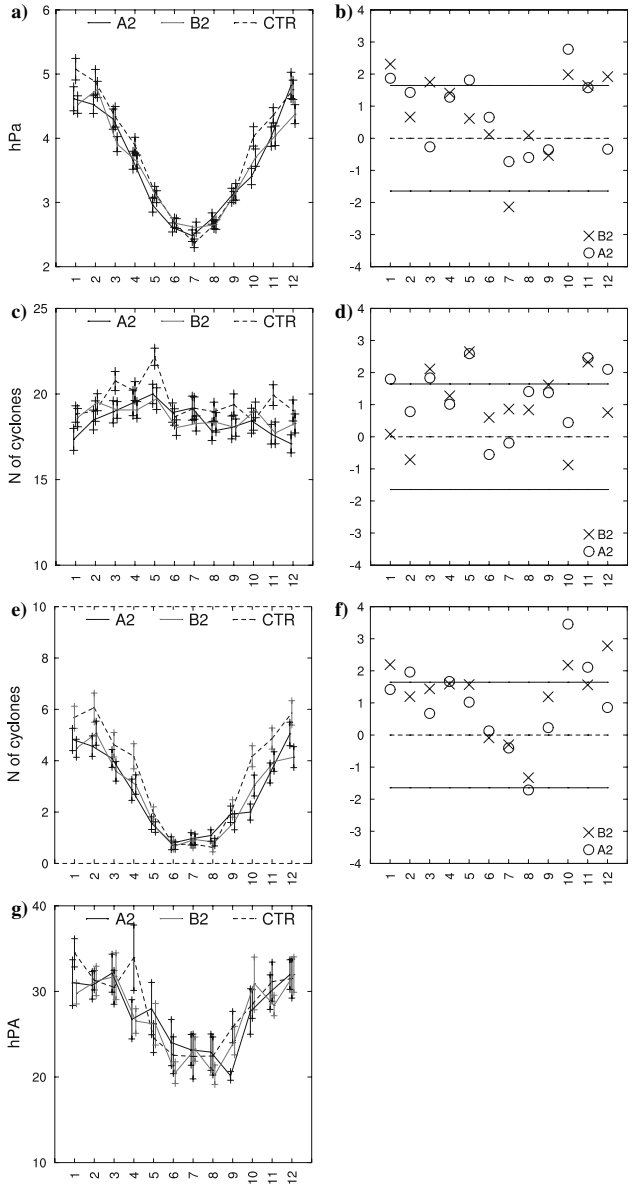

Fig. 16 Same as previous Fig. 15, except that the results for the RUS region are shown

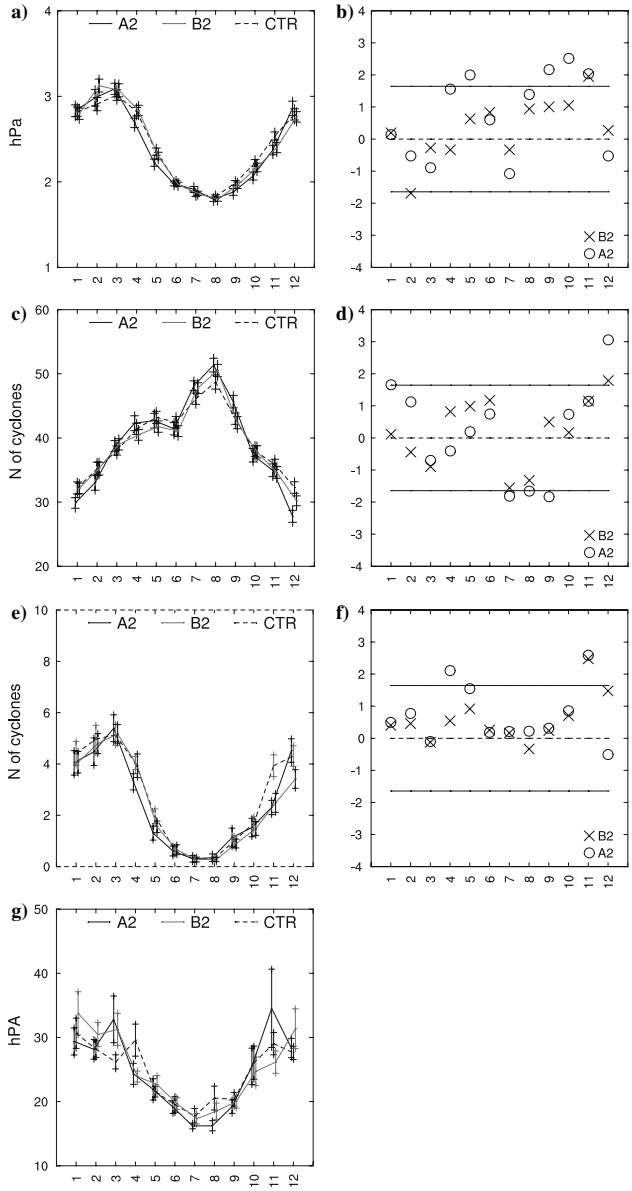

Fig. 17 Same as previous Fig. 15, except that the results for the CEM region are shown

and Christoph 1999). This shift is due to a northward shift of the descending branch of the Hadley cell, which follows the larger warming of the upper tropophere in the tropics than at mid-latitudes. The decrease of cyclones in summer over the NEA region is consistent with the increased frequency of blocking-like circulation patterns over the northwest Atlantic (Pal et al. 2004), which tends to deflect storms north of the European region, leading to generally drier conditions and lower storminess.

In summary, this study suggests a winter intensification of cyclonic activity and extreme cyclones over northwestern Europe and an attenuation of events over southern and eastern Europe. These changes appear to be consistent with trends already detected during the second half of the twentieth century (e.g., Pal et al. 2004; Trigo 2005; Lionello et al. 2006a; Wang et al. 2006). The overall number of cyclones is projected to mostly decrease, a trend also observed during recent decades over southern Europe (Trigo 2005). The meaning of this reduction, which is opposite to the increase of the synotic signal, is not clear, possibly pointing to a change of the conditions triggering cyclogenesis and to a suppression of weak disturbances over most of Europe.

Finally, this study suggests a number of general considerations. A regional characterization of changes in cyclonic activity and synoptic variability over Europe is

important, as quite different behaviors can be found at relatively small spatial scales. Intermonthly variability can be pronounced and the separation of internal variability from the climate change signal remains a fundamental issue. In addition, the changes in statistics of intense events can depend considerably on the intensity threshold considered, which calls for a careful analysis of the intensity distribution of cyclones.

References

Alexander LV, Tett SFB and Jonsson T (2005) Recent observed changes in severe storms over the United Kingdom and Iceland. Geophys Res Lett 32:L13704

Alexandersson H, Schmith T, Iden K, Tuomenvirtas H (2000) Trends in storms in NW Europe derived from an updated pressure data set. Clim Res 14:71–73

Barring L, Von Storch H (2004) Scandinavian storminess since about 1800. Geophys Res Lett 31:L20202. doi:10.1029/2004GL020441

Giorgi F, Marinucci MR, Bates GT (1993a) Development of a second generation regional climate model (REGCM2). Part I: boundary layer and radiative transfer processes. Mon Weather Rev 121:2794–2813

Giorgi F, Marinucci MR, Bates GT, DeCanio G (1993b) Development of a second generation regional climate model (REGCM2). Part II: convective processes and assimilation of lateral boundary conditions. Mon Weather Rev 121:2814–2832

Giorgi F, Bi X, Pal JS (2004a) Mean, interannual variability and trends in a regional climate change experiment over Europe. Part I: present day climate (1961–1990). Clim Dyn 22:733–756

Giorgi F, Bi X, Pal JS (2004b) Mean, interannual variability and trends in a regional climate change experiment over Europe. Part II: future climate scenarios (2071–2100). Clim Dyn 23:839–858

Hurrell JW (1995) Decadal trends in the North Atlantic oscillation: regional temperatures and precipitation. Science 269:676–679

Jones RG, Murphy JM, Hassell D, Taylor R (2001) Ensemble mean changes in a simulation of the European mean climate of 2071–2100 using the new Hadley centre regional modeling system HadAM3H/HadRM3H. Hadley Centre report, 19 p

Kaas E, Flather R, Lionello P, Malguzzi P, Reistad M, de Ronde JS, von Storch H (2001) STOWASUS 2100: regional storm wave and surge scenario for the 21st century, available at http://web.dmi.dk/pub/STOWASUS-2100/Final/Synthesis.pdf

Kalnay E, Kanamitsu M, Kistler R, Collins W, Deaven D, Gandin L, Iredell M, Saha S, White G, Woollen J, Zhu Y, Chelliah M, Ebisuzaki W, Higgins W, Janowiak J, Mo KC, Ropelewski C, Wang J, Leetmaa A, Reynolds R, Jenne R, Joseph D (1996) The NCEP/NCAR 40-year re-analysis project. Bull Amer Meteor Soc 77:437-471

Leckebusch G, Koffi B, Ulbrich U, Pinto J, Spangehl T, Zacharias S (2006) Analysis of frequency and intensity of European winter storm events from a multi-model perspective, at synoptic and regional scales. Clim Res 31:59–74

Lionello P (2005) Extreme surges in the Gulf of Venice. Present and future climate. In: Fletcher C, Spencer T (eds) Venice and its lagoon, state of knowledge. Cambridge University Press, Cambridge, pp 59–65

Lionello P, Sanna A (2005) Mediterranean wave climate variability and its links with NAO and Indian monsoon. Clim Dyn 26:611–623. doi:10.1007/s00382-005-0025-4

Lionello P, Dalan F, Elvini E (2002) Cyclones in the Mediterranean region: the present and the doubled CO_2 climate scenarios. Clim Res 22:147–159

Lionello P, Elvini E, Nizzero A (2003) Ocean waves and storm surges in the Adriatic Sea: intercomparison between the present and doubled CO_2 climate scenarios. Clim Res 23:217–231

Lionello P, Bhend J, Buzzi A, Della-Marta PM, Krichak S, Iansà A, Maheras P, Sanna A, Trigo IF, Trigo R (2006a) Cyclones in the Mediterranean region: climatology and effects on the environment. In: Lionello P, Malanotte-Rizzoli P, Boscolo R (eds) Mediterranean climate variability. Elsevier, Amsterdam, pp 324–372

Lionello P, Malanotte-Rizzoli P, Boscolo R, Alpert P, Artale V, Li L, Luterbacher J, May W, Trigo R, Tsimplis M, Ulbrich U, Xoplaki E (2006b) The Mediterranean climate: an overview of the main characteristics and issues. In: Lionello P, Malanotte-Rizzoli P, Boscolo R (eds) Mediterranean climate variability. Elsevier, Amsterdam, pp 1–26

Lionello P, Cogo S, Galati MB, Sanna A (2007) Wind wave climate change in the Mediterranean. Glob Planet Change (in press)

Maheras P, Flocas H, Patrikas I, Anagnostopoulou C (2001) A 40 year objective climatology of surface cyclones in the Mediterranean region: spatial and temporal distribution. Int J Climatol 21:109–130

Nakićenović N, Alcamo J, Davis G, de Vries B, Fenhann J, Gaffin S, Gregory K, Grabler A, Jung TY, Kram T, La Rovere EL, Michaelis L, Mori S, Morita T, Pepper W, Pitcher H, Price L, Raihi K, Roehrl A, Rogner HH, Sankovski A, Schlesinger M, Shukla P, Smith S, Swart R, van Rooijen S, Victor N, Dadi Z (2000) IPCC special report on emissions scenarios. Cambridge University Press, Cambridge, 599 p

Pal JS, Small EE, Eltahir EAB (2000) Simulation of regional—scale water and energy budgets: representation of subgrid cloud and precipitation processes within RegCM. J Geophys Res 105:29579–29594

Pal JS, Giorgi F, Bi X (2004) Consistency of recent European summer precipitation trends and extremes with future regional climate projections. Geophys Res Lett 31:L13202. doi:10.1029/2004GL019836

Pinto JG, Spangehl T, Ulbrich U, Speth P (2006a) Assessment of winter cyclone activity in a transient ECHAM4-OPYC3 GHG experiment. Meteorol Zeitschrift 15:279–291

Pinto JG, Spangehl T, Ulbrich U, Speth P (2006b) Sensitivities of a cyclone detection and tracking algorithm: individual tracks and climatology. Meteorol Zeitschrift 14:823–838

Simmons AJ, Gibson JK (2000) The ERA-40 Project Plan, ERA-40 Project Report Series n.1. ECMWF, Reading, 62 p

Trigo IF (2005) Climatology and interannual variability of storm-tracks in the Euro-Atlantic sector: a comparison between ERA-40 and NCEP/NCAR reanalyses. Clim Dyn 26:127–143. doi:10.1007/s00382-005-0065-9

Ulbrich U, Christoph M (1999) A shift in the NAO and increasing storm track activity over Europe due to anthropogenic green house gas. Clim Dyn 15:551–559

Von Storch H, Zwiers FW (1999) Statistical analysis in climate research, Cambridge University Press, Cambridge, 499 p

Wang XL, Swail VR (2001) Changes of extreme wave heights in Northern Hemisphere oceans and related atmospheric circulation regimes. J Clim 14:2204–2221

Wang XL, Swail VR (2002) Trends of Atlantic wave extremes as simulated in a 40-year wave hindcast using kinematically reanalyzed wind fields. J Clim 15:1020–1035

Wang XL, Swail VR (2006) Climate change signal and uncertainty in projections of ocean wave heights. Clim Dyn 26:109–126

Wang XL, Swail VR, Zwiers FW (2006) Climatology and changes of extra-tropical cyclone activity: comparison of ERA-40 with NCEP/NCAR reanalysis for 1958–2001. J Clim 19:3145–3166

WASA Group (1998) Changing waves and storms in the North East Atlantic? Bull Am Met Soc 79:741–760